Intermetallic particles trigger streaking corrosion in AA7075-T6

Mopon, M.; Mol, J.M.C.; Garcia, Santiago J.

Important note
To cite this publication, please use the final published version (if applicable).
Please check the document version above.

Article

Intermetallic particles trigger streaking corrosion in AA7075-T6

Check for updates

Marlon Mopon Jr.[1,2] ✉, Arjan Mol[3] & Santiago J. Garcia[1] ✉

Streaking corrosion (SC) of AA7075-T6, characterized by the rapid dissolution of an altered surface layer (ASL) formed through mechanical surface treatments, is investigated. Utilizing in situ high-resolution reflected light microscopy, we reveal that SC initiates preferentially on intermetallic particles (IMP) or pre-existing pits. Optical evidence of galvanic interactions between propagating streaks and connected IMPs is observed. Concurrent in situ open circuit potential (OCP) measurements show a characteristic pattern that correlate with SC initiation, progression, and termination. This work demonstrates the effectiveness of a simple in situ optical-electrochemical setup in tracking dynamic local corrosion processes and directly linking OCP transients to specific corrosion events.

AA7075 is an Al-Zn-Cu-Mg alloy commonly used in the aerospace industry due to its good strength to weight ratio. The microstructure that arises from its composition, however, is prone to local corrosion. Intermetallic particles (IMPs) formed due to the presence of alloying elements undergo a complex dealloying process that eventually lead to micro-galvanic coupling with the bulk matrix[1,2]. Typical AA7075 IMPs include S-phases (Al_2CuMg), θ-phases (Al_2Cu), and secondary particles, of which Al_7Cu_2Fe, $(Al,Cu)_6(Fe,Cu)$, and $MgSi_2$ are most abundant[3,4]. Local corrosion of S- and θ-phase IMPs begins with a dealloying process wherein less noble IMP components such as Mg and Al are dissolved[5,6]. This leads to enrichment of the Cu at the IMP which facilitates oxygen reduction reaction and triggers anodic dissolution of the less noble adjacent matrix (i.e., trenching). Meanwhile, some secondary particles (e.g., Al_7Fe_2Cu[7]) have been shown to be more electrochemically stable and thus may undergo slower and limited dealloying. Their local corrosion behaviour is characterized by less extensive dealloying although still accompanied by trenching[7,8]. Presence of grain boundary precipitates and precipitate-free zones in the AA7075 grain boundaries also lead to intergranular corrosion susceptibility[9,10].

Apart from the corrosion susceptibility due to its microstructure, mechanical surface treatments of the AA7075 surface (e.g., abrading, machining, polishing) can also render it vulnerable to a form of altered surface layer (ASL) attack[11–14]. This ASL attack is similar in nature to reported corrosion of near surface deformed layers (NSDL) present in aluminium alloys[15–19]. Notably, majority of these works studied NSDL in the context of filiform corrosion which occurs when the aluminium alloy is covered with an organic coating. The ASL's (or NSDL's) vulnerability has been attributed to redistribution of active alloying elements (i.e., Zn, Mg) from precipitates and IMPs into the ASL due to high shear straining during surface polishing[20]. Huang et al.[12,21] referred to a form of this ASL attack as

streaking corrosion due to characteristic streaks formed by its preferential propagation along abrasion grooves. Streak propagation is thought to be driven by the low pH produced by corrosion product hydrolysis. The low pH undermines passivity and pushes the streak front forward[12]. The topology of the grooves provide an ideal containment system for this low pH environment leading to the observed preferential propagation at these locations. Other aluminium alloys such as AA8006[12] and AA7055[11,22] have also exhibited similar streaking behaviour.

Nevertheless, there are still questions regarding initiation and propagation of streaking corrosion in the ASL. Zhao and Frankel proposed that the initiation sites for ASL attack in AA7075 during polarized conditions are active nano-grain boundaries enriched with Zn and Mg[20]. This does not account though for the highly localized occurrence of streaking corrosion especially during open circuit conditions. In this work, we used an in situ optical-electrochemical technique to deepen and clarify our understanding of the initiation and propagation of streaking corrosion in AA7075-T6 microelectrodes. The technique utilizes reflected light microscopy with high spatial and temporal resolution to monitor changes on the surface. When coupled with open circuit potential (OCP) measurements, determination of the electrochemical signals of specific corrosion events on the surface is possible. Furthermore, scanning electron microscopy (SEM) and energy-dispersive x-ray spectroscopy (EDX) was also utilized in order to identify features that likely contribute to initiation of streaking corrosion.

Results

Streaking corrosion initiation

Figure 1 shows that local corrosion processes on the surface of a roughly-polished AA7075-T6 sample (i.e., sample with visible grooves from grinding) can generally be divided into two types: (1) dealloying and trenching

---

[1]Aerospace Structures and Materials Department, Delft University of Technology, Delft, the Netherlands. [2]Department of Chemical Engineering, University of the Philippines Diliman, Quezon City, Philippines. [3]Department of Materials Science and Engineering, Delft University of Technology, Delft, the Netherlands. ✉e-mail: m.mopon@tudelft.nl; s.j.garciaespallargas@tudelft.nl
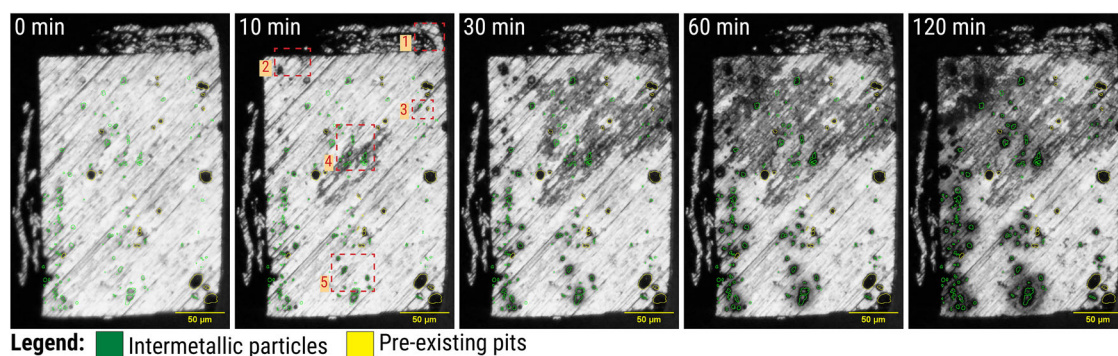
Fig. 1 | Evolution of local corrosion on a rough-polished AA7075 observed by in situ microscopy. In situ reflected light microscopy images of an AA7075 surface exposed to 0.05 M NaCl at OCP show the evolution of local corrosion processes such as streaking corrosion (area 1–4), and IMP dealloying and trenching (area 5). The microstructure map which indicates the location of IMPs and pre-existing pits shown in this figure was created from post-immersion SEM images. The legend indicates the boundary colour for IMPs and for pre-existing pits.

Fig. 2 | Affected area vs. time of Fig. 1 sample. Affected area curve shows majority of the area that changed can be attributed to the propagation of streaking corrosion.
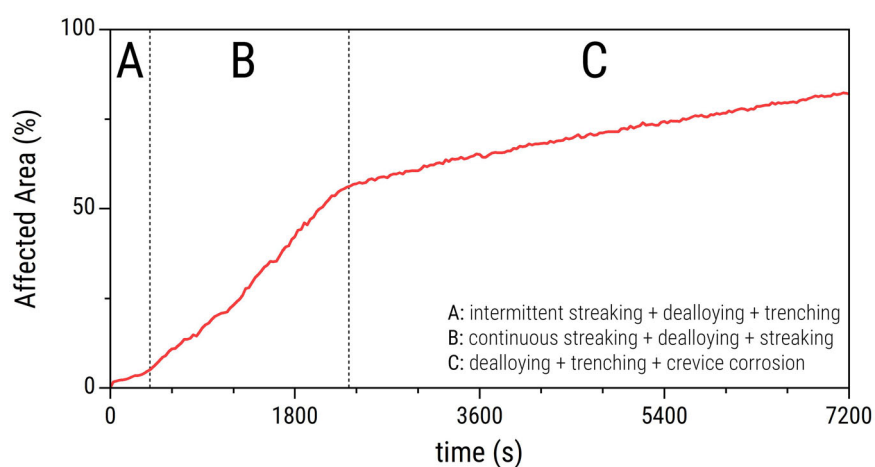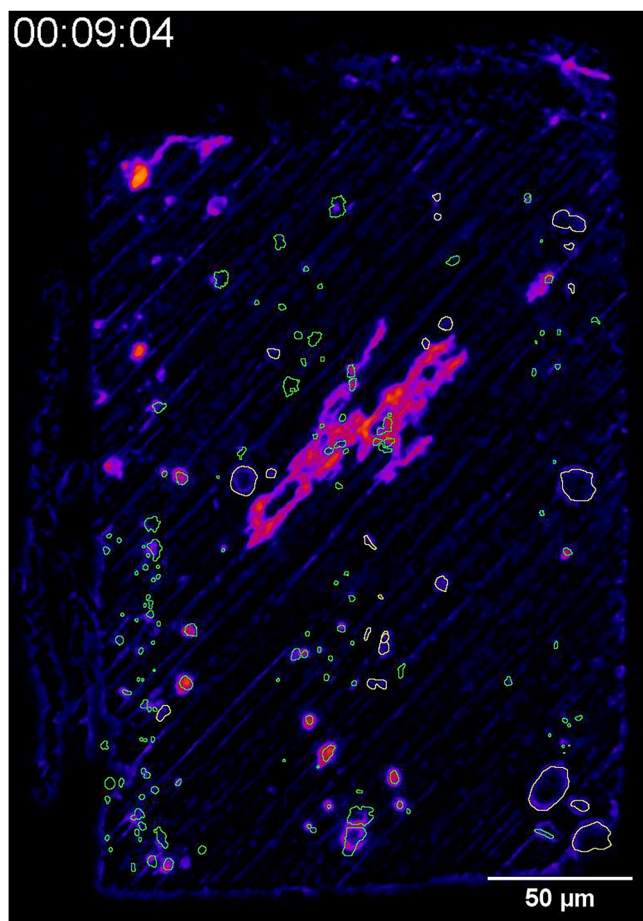
around IMPs and (2) streaking corrosion on the bulk matrix. Dealloying is observed optically as surface darkening within the IMP boundaries (i.e., green boundaries) while trenching is the subsequent darkening of the matrix adjacent to the IMP boundaries[23,24]. The IMPs in area 5 of the microscopy image at 10 minutes (Fig. 1) exhibit this behaviour. Majority of the IMPs showed signs of dealloying during the first 10 minutes of exposure. Gradual trenching around the dealloyed IMPs progressed for the rest of the immersion. The image of the surface at 120 minutes shows extensive IMP dealloying and trenching. However, their effect does not extend too far from the IMP boundary.

Streaking corrosion was observed as dark lines that generally grew along the direction of the abrasion grooves. The streaks initiated on four separate locations (areas 1–4 in Fig. 1) within the first 10 minutes of immersion. Areas 1, 2, and 3 each exhibited one streaking initiation event, while Area 4 showed four. The area 4 streaks propagated the most and covered almost half of the sample surface within 60 minutes of immersion. Visual appearance of the streaked surfaces are consistent with optical micrographs of streaking corrosion by Huang et al.[12] and of ASL attack shown by Wang et al.[11,25] The extent of streaking corrosion propagation can be further quantified with the affected area – a measure of the percentage of pixels in the subtracted images which exhibited gray level changes greater than or equal to a threshold. The affected area curve for this sample (Fig. 2) shows that the continuous streaking corrosion from 5 until around 40 minutes of exposure indeed led to rapid surface changes. The increasing part of the curve shows staircase-like features consistent with the incremental propagation of streaking corrosion. This incremental propagation

suggests that the overall streaking is a sequence of smaller initiation-propagation-termination events.

Figure 3 shows the time-evolution of the surface activity maps, where streaking corrosion appears as fast-spreading purple lines that extend into the matrix. It provides a clearer view of streaking in Areas 1, 2, and 3 and indicates that the streak in Area 2 and Area 3 likely originated from IMPs. Figure 3 also shows that the activity in area 4 started with four individual streaks. Activity maps in Fig. 4 are still frames from Fig. 3 which show initiation and subsequent growth of the streaks. It is interesting to point out that the four streaking events did not happen at the same time. Instead, one streak initiates, propagates, and ends before another streak begins from a different location. This gives the overall impression of incremental streaking propagation shown in Fig. 2. The first streak initiated at around 41 seconds from start of immersion (Fig. 4a). The initiation site was on the right edge of particle P1, an S-phase IMP based on the post-mortem EDX analysis (Supplementary Fig. S1). The streak followed a groove and propagated towards the top right direction. The streaking ended at around 54 s. The second streak initiated at the left edge of P2 (S-phase, EDX in Supplementary Fig. S2) and propagated towards the bottom left direction (Fig. 4b). It is noted that P2 showed signs of increasing activity on the IMP surface before the initiation of the streak. The streak front advanced through a well defined groove at 153 s and covered a distance of around 9 μm. Its estimated front speed of 4.5 μm s^{-1} is consistent with streak rate reported by Huang et al.[12] At 158 s, the streak connected to a nearby IMP (P') which then showed signs of activation and activity spread both along and lateral to the grooves in its vicinity (indicated by the dashed arrows in the activity map at

Fig. 3 | Time-lapse video of local corrosion of roughly-polished AA7075 sample.
Evolution of surface changes on roughly-polished AA7075 sample during the first
10 minutes of immersion in 0.05 M NaCl (In the PDF version of this article, please
click anywhere on the figure or caption to play the video in a separate window).

The RM image of the surface at the end of immersion (Fig. 6a) shows that, in the absence of deep grooves, streaking corrosion has a patchy texture. The edges of these streaking patches are also more billowing and less sharp. A video depicting the evolution of activity of the overall surface is provided in Fig. 7. The video highlights that the hallmark of streaking corrosion—rapid spreading across the surface—is still observed even on a smoother sample. This fast-spreading behaviour indicates that the corrosion events seen on smoothly-polished surfaces are the same as those occurring on roughly polished samples, despite the differences in morphology.

The overall streaking at the end of immersion of the smoothly-polished sample was traced to areas 6 and 7 in Fig. 6a. Activity maps in Fig. 6b and c are still frames from Fig. 7 and show the initiation and first couple of seconds of propagation of streaks in area 6. It is evident from the maps that the streaks originated from P4 and P5, both of which are S-phase particles (EDX analyses in Supplementary Figs. S4 and S5). The streak originating from P4 (Fig. 6b) started at its edge and propagated in a diffused manner with a linear propagation speed (~ $2 \mu s^{-1}$). This value is comparable to that observed from the rough sample. Streaking terminated at around 163 s. Similar to P2, P4 exhibited signs of increase activity on the IMP surface before the onset of streaking. The streak originating from P5 (Fig. 6c) started on the IMP surface and then rapidly propagated to the surrounding matrix until it terminated at around 197 s. The surface was inactive prior to streak initiation. It should be noted that another streak initiates from P5 later on, at around 211 s. Figure 6d and e presents streaking initiation sites in area 7. Unlike the previous streaking events, the ones observed in this area are associated with pits and not IMPs. Pre-immersion SEM (Supplementary Fig. S6) confirmed the presence of a pit on the same location as the initiation site of the streak in Fig. 6d. Meanwhile, post-immersion SEM (Supplementary Fig. S7) confirmed the presence of a pit at Fig. 6e streak initiation site. Streak propagation from these pits were similar in behaviour to streak propagation from IMPs. Interestingly, all the streaks initially spread to bigger areas relative to their in-groove counterparts within the same time period. Despite this, the fraction of the surface affected by streaking corrosion is visibly less than that of the roughly-polished AA7075-T6.

Post-immersion secondary electron images (Fig. 8a) indicate that the patchy texture of streaking corrosion arise from a mix of dissolved and undissolved sections. Bright spots on the dissolved areas also point to exposure of IMPs or dispersoids during ASL dissolution. Exposure of these bright spots is most apparent on the areas traversed by streaking corrosion and not on the intact areas. Post-immersion EDX analysis of streaked and unstreaked areas (Fig. 8b) from another smoothly-polished replicate (Supplementary Discussion) was also conducted to investigate possible compositional difference. It is noted that streaking corrosion in this replicate initiated from Fe-rich IMPs (Supplementary Discussion). The resulting EDX maps of the streaked areas revealed no discernible differences between the two areas. This may indicate either that a thin ASL is present on the unstreaked area but falls below the detection limit, or that all ASL material susceptible to streaking is localized to the streaked area and has been entirely removed by corrosion. The absence of detectable differences further suggests that the streaking does not result in the accumulation of substantial corrosion products on the affected surface. Instead, the dissolved metal is likely retained in the solution or redeposited beyond the analysed region. While the observed morphological differences between roughly and smoothly polished surfaces may provide additional insight into the nature of streaking corrosion, a more detailed investigation is outside the scope of this work and is recommended for future study.

Notably, among 28 streaking initiation events across three smoothly-polished samples and one roughly-polished sample, 21 originated from intermetallic particles (i.e., 6 from the sample shown in Fig. 1 sample, 2 from the sample in Fig. 6, 8 from the replicate in Figs. S10, 5 from the replicate in Fig. S14). This indicates that 75 percent of streaking corrosion events can be traced to IMPs and suggests that these particles can act as trigger for streaking corrosion in AA7075. The rest of the streaking corrosion events can potentially be attributed to initiation from pits as shown in Fig. 6d and e.

160 s). With further exposure, more active zones appeared near P'. This streaking ended at around 171 s. Figure 4c shows that the third streak started at the bottom edge of P3 (S-phase, EDX in Supplementary Fig. S3) at 194 s. The streak front moved towards the top right direction and then connected to a low activity patch. This patch showed gradual increase of activity from 199 s until its apparent termination at 209 s but triggered no immediate activity spread. The fourth streak initiated at the top edge of P3, right where a smaller IMP is located (Fig. 4d). The composition of the smaller IMP was not confirmed experimentally but based on its proximity to a cluster of S-phases, it is likely to have same composition. The streak also moved towards the top right direction where it then connected with the active patch from the third streak. This lead to activity spread that headed back to P3, connected with the third streak, and then continued on as a streak front from the left edge of the IMP cluster below P3. All other streaking events during the immersion period can be traced to sites connected to the propagation of the fourth streak. Despite the large area affected by streaking corrosion, the affected depth appears to be relatively shallow. This is evident in the end-of-immersion activity map for area D (Fig. 5a) which shows that the activity level of the streaks remained in the low level (purple in the colour scale) while that of the trenches reached a higher activity level (yellow-orange in the colour scale). The post-mortem secondary electron image (Fig. 5b) also shows distinct trenches around the IMPs but not so visible streak morphology.
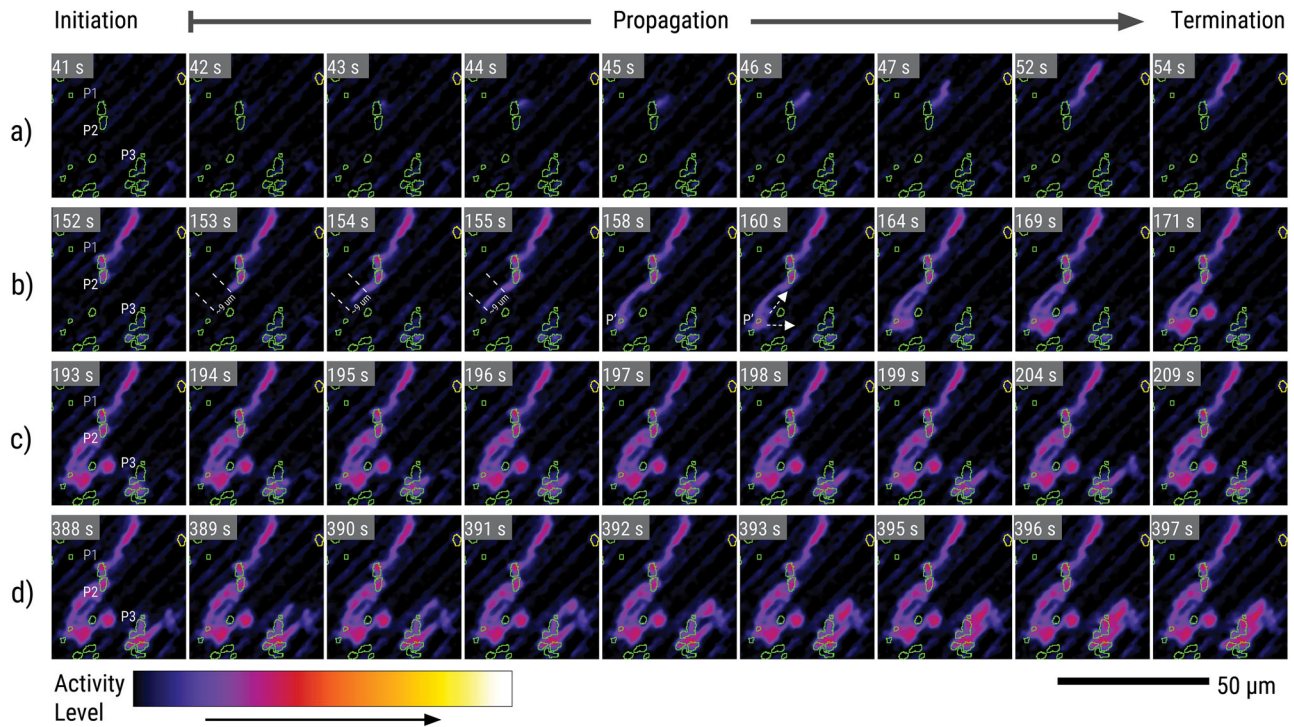
Analysis of the local corrosion behaviour in a smoothly-polished AA7075-T6 surface (i.e., sample with no visible grooves from grinding) was conducted to better understand streaking not confined to abrasion grooves.

Fig. 4 | Local activity maps showing streak initiation in Fig. 1 sample. Activity maps from area D in Fig. 1 show the initiation of four streaks (**a–d**) which eventually propagated to the rest of the sample surface. The activity maps were obtained by subtracting from the image at $t = 0$ s and without applying any threshold.

Fig. 5 | Activity at end of immersion and corresponding morphology observed with post-immersion SEM. a Activity map of area D at end of immersion and its (**b**) post-mortem secondary electron image. The high activity around the particles (orange-yellow zones) indicate extensive surface change due to trenching. Streaked areas (purple zones) have shallow dissolution and do not stand out in the post-mortem electron image.
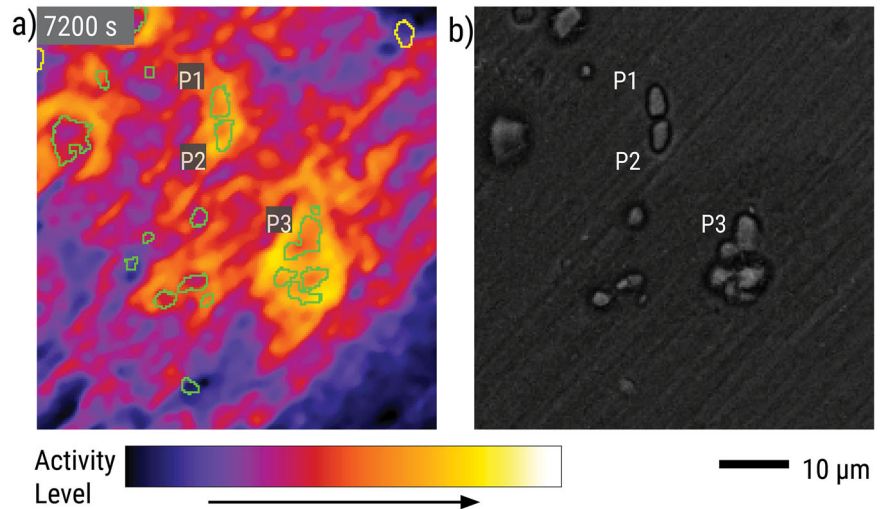

Surface activation of IMPs that initiate and do not initiate streaks

The preceding section shows that streaking corrosion mostly initiates on IMPs and to certain extent, pre-existing defects. However, majority of the IMPs on the samples analysed did not serve as initiation sites of streaking corrosion. Local activity of the streak-initiating IMPs was further scrutinized to see if there are any characteristic differences between them and the other IMPs. This was achieved by looking at the activation of the IMP surfaces through their corresponding simplified pixel activity level distribution (sPADs). The sPADs present the maximum (maxAL), median (midAL), and minimum (mindAL) activity level of the pixels that are within the IMP surface boundary as a function of time.

N1 (Fig. 9a) is an IMP from the test shown in Fig. 1 and N2 (Fig. 9e) is an S-phase from the test shown in Fig. 6 (EDX analyses in Supplementary Figs. S8 and S9). Both of these IMPs did not initiate streaking corrosion. Similar to S-phase sPADs in our previous work[24], the onset of changes for

the pixels inside the IMP boundaries of N1 and N2 were within 60 seconds from the start of exposure to the electrolyte. Average activation onset time for known S-phase particles that did not initiate streaking ($n = 13$) from the smoothly-polished sample is 13.1 ± 4.7 s. Based on the midAL curve, the particles also exhibited an initial fast period of midAL increase followed by a slow period, both of which showed generally smooth features (i.e., no discontinuities). The midAL increase during the fast period is associated with the rapid dealloying of the IMP[23,24]. Once the particle has dealloyed substantially, transition to the slow period is observed. This period is associated with trenching around the IMP[23,24]. The activity maps in the insets show that the changes for N1 and N2 are characterized by gradual spread on the IMP surface. It is noted that the kink at around 45 seconds visible in the N2 midAL curve is due to a change in focus of the microscope during image acquisition. This is also seen in the other sPADs from the same trial (i.e., P4) and is not regarded as information on surface phenomena.
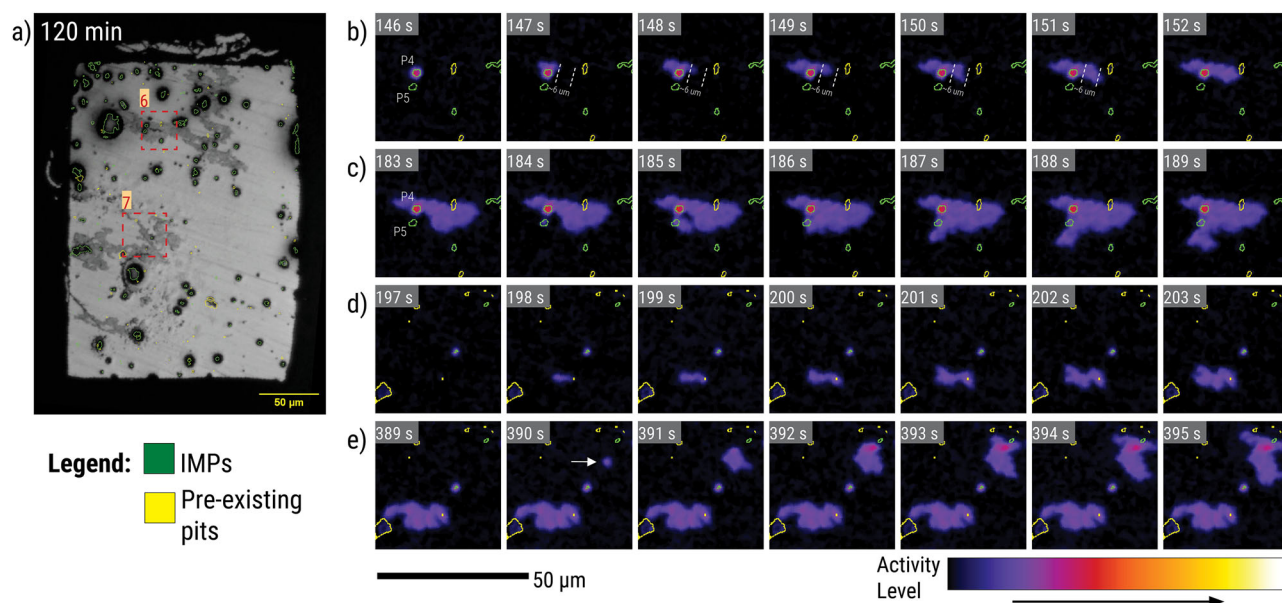
Fig. 6 | Overall streaking corrosion and local streak initiation in a smoothly-polished sample. In situ reflected light microscopy image (**a**) of a polished AA7075 surface exposed to 0.05 M NaCl at OCP shows the extent of streaking corrosion in the absence of deep abrasion grooves. Activity maps show streaking initiation sites in (**b**, **c**) area 6, and (**d**, **e**) area 7. The activity maps were obtained by subtracting from the image at $t = 0$ s and without applying any threshold. The microstructure map overlay was created from pre-immersion SEM mapping. The legend indicates the boundary colour for IMPs and for pre-existing pits.
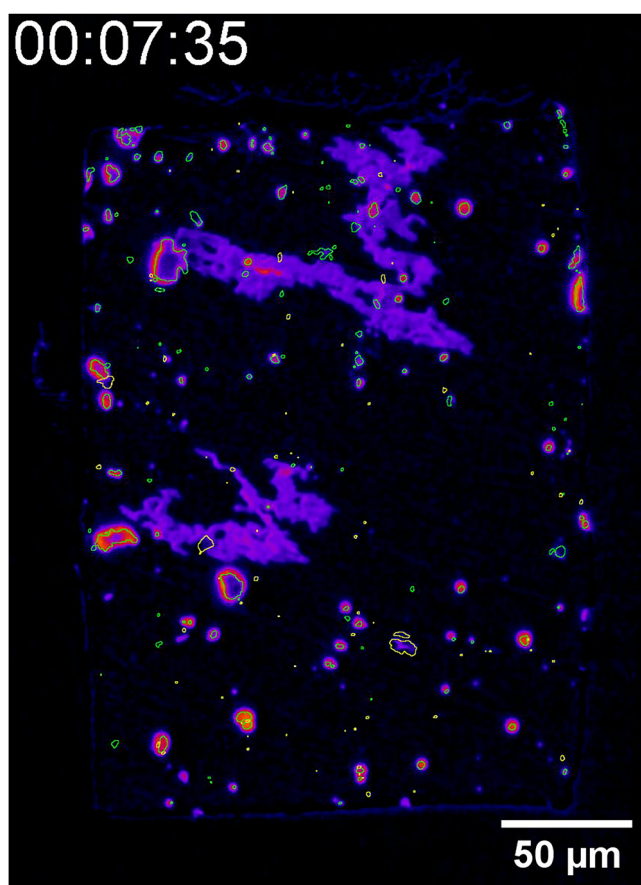

Fig. 7 | Time-lapse video of local corrosion of smoothly-polished AA7075 sample. Evolution of surface changes on smoothly-polished AA7075-T6 sample during the first 15 minutes of immersion in 0.05 M NaCl (In the PDF version of this article, please click anywhere on the figure or caption to play the video in a separate window).

Majority of the streak-initiating IMPs (i.e., P1, P2, P3, P5) show IMP surface activation profiles different to those from the non-initiating IMPs reported here and in previous works[23,24]. P1 sPAD (Fig. 9b) registered a maxAL step increase at around 42 s due to streak initiation from its right edge. A gradual rise in activity from 54 s suggests surface dealloying, coincide with the end of streaking corrosion shown in Fig. 4a. The activity increase during the apparent dealloying (54–70 s on the midAL curve) resembles typical S-phase behaviour but eventually plateaued at an activity level of around 25. Inset activity maps reveal this plateau is due to inactivity on parts of the IMP surface near the left and bottom edges, likely caused by compositional variation. Nonetheless, midAL step increases at 134 s and 149 s (see black arrow in Fig. 9b) indicate that these eventually registered activity consistent with streaking.

P2 activation (Fig. 9c), marked by dealloying around 98 s, occurred before any streaking linked to the particle but significantly after typical S-phase activity onset. Its dealloying progressed more slowly than non-initiating IMPs. For reference, N1's midAL rose by 8 levels in 10 s (75–85 s), while P2 increased by only 3 over a similar period (100–110 s). A distinct midAL step increase at ~120 s (see black arrow in Fig. 9b) signals a brief streaking event directly over the IMP surface.

Although the P3 sPAD (Fig. 9d) shows a midAL increase at around 60 s, its almost flat maxAL suggests that the midAL increase might be due to an image subtraction artefact caused by scratches on the area and not due to actual changes on the IMP surface. Visible change in the maxAL trend at around 180 s indicates that this might be the actual IMP activation. Again, the activity step increase also suggests that the activation is due to streaking over the IMP, similar to that seen in P2. Changes in the upper section of the P3 attributed to dealloying is observed at around 286 s.

Among the IMPs in Fig. 6 associated with streaking corrosion initiation, only P4 exhibited an initial activation profile comparable to that of a typical S-phase IMP (Fig. 9f). Its activation onset at 13 seconds is consistent with a dealloying particle. Slow down of activity increase associated with trenching is observed after 60 s. At 147 s, streak initiation from the trench is observed as an instantaneous increase in the maxAL and midAL. It is noted that only one other particle in the replicate tests (Supplementary Discussion) exhibited similar behaviour to P4.
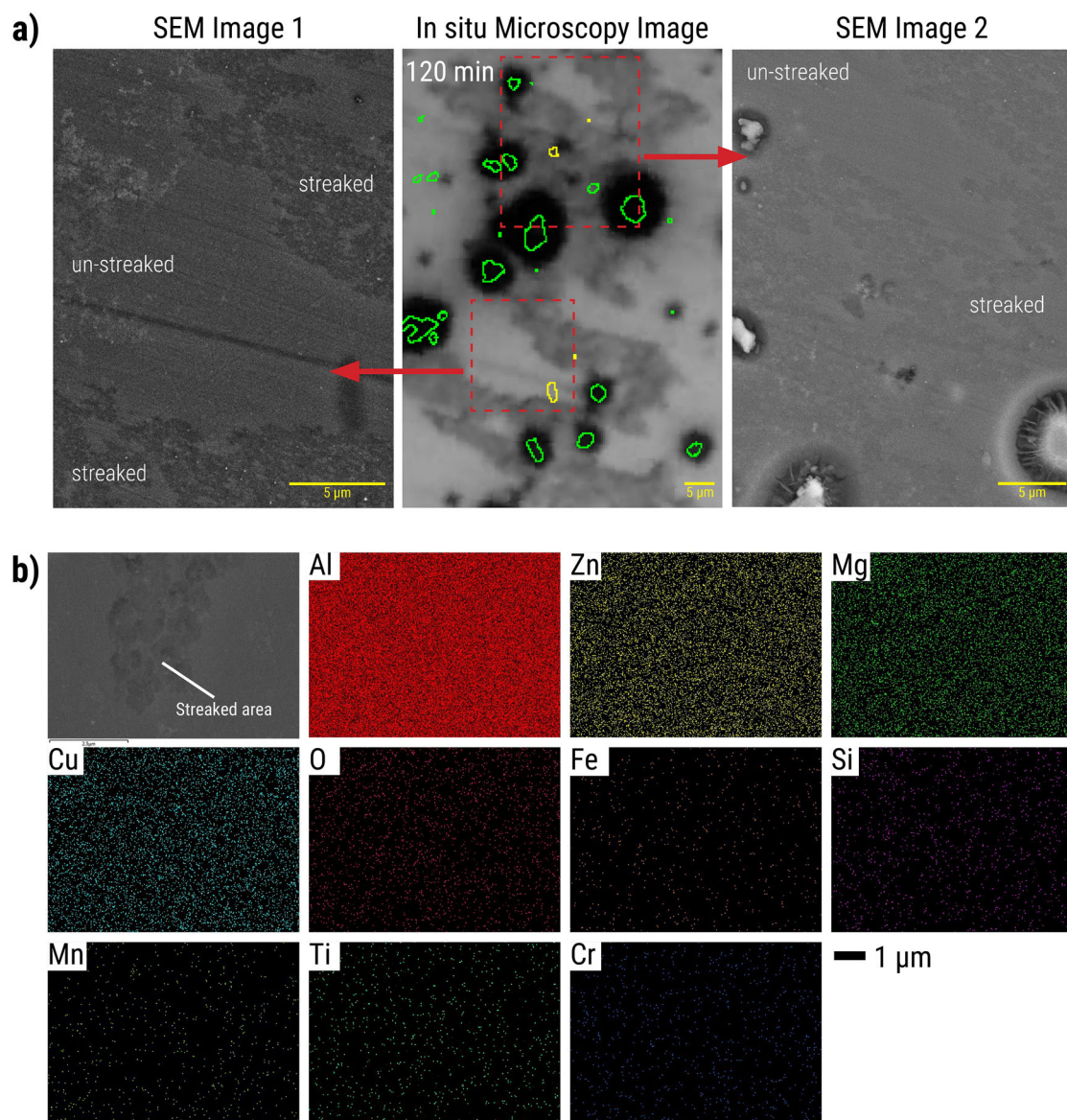
Fig. 8 | Post-immersion SEM-EDX analysis of streaked and unstreaked areas from smoothly-polished samples. a In situ microscopy image of streaking corrosion and post-immersion secondary electron images of the streaking corrosion patches show the corroded areas are composed of dissolved and undissolved sections. The images also show that the depth of streaking is visibly less than trenching around intermetallic particles. **b** Post-immersion EDX mapping of streaked areas show no detectable difference compared to the unstreaked areas.

Lastly, P5 activation onset (Fig. 9g) occurred much later than typical S-phase onset. The IMP surface activation is characterized by a jump in the sPAD attributed to streaking over the IMP surface. This also quickly transitioned to streaking corrosion outside the IMP as seen in the inset. The midAL following the sPAD jump is lower than the values seen in the non-initiating IMPs.

Intermetallic particle activity and streak propagation

The sPADs in Fig. 9 highlighted generally non-typical activation of IMPs that initiated streaking corrosion. Interestingly, they also show that when an IMP is involved in streaking, step-discontinuities appear on its sPAD at the time of streaking initiation. The sPADs also exhibit near-horizontal profiles for the maxAL, midAL, and minAL during streak propagation. This behaviour points to temporary arrest of IMP activity during streak propagation. Extended sPADs of the IMPs (Fig. 10b–d, f, g) involved with streaking corrosion show that their activity increase eventually resumed. This activity increase resumption is generally visible with the entire sPAD

but is easiest seen with the minAL. The activity arrest is not limited to IMPs where streaking corrosion initiated. Figure 11 shows activity maps of two active particles (indicated by solid white arrow in the 600-s frame of Fig. 11a and the 250-s frame of Fig. 11b) activation profiles similar to the non-initiating IMPs. However, during the immersion, propagating streaks (indicated by dashed white arrow in the 1800-s frame of Fig. 11a and the 285-s frame of Fig. 11b) eventually linked with the surface of these IMPs (i.e., streak-linked IMPs). Their corresponding sPADs showed a transition to near-horizontal profiles at the time of connection (see 1980-s frame of Fig. 11a and 292-s frame of Fig. 11b). As with the streak-initiating IMPs, activity increase of streak-linked IMPs eventually resumed.

Activity increase resumption for the particles involved with the streaks was observed to be related to the overall streaking termination. For the roughly-polished sample, the termination occurred at around 40 minutes of exposure (Fig. 2). The activity resumption for all the streak-initiating (Fig. 10b–d) and streak-linked (Fig. 11a) IMPs happened after this time. Streak-initiating and streak-linked IMPs from the smoothly-polished sample also
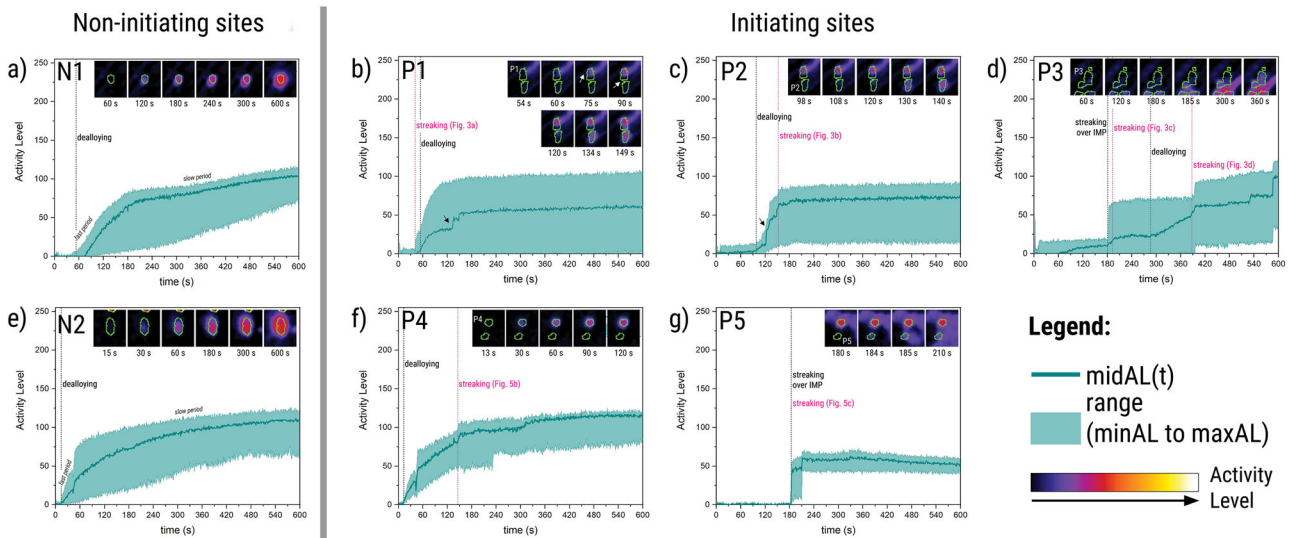
Fig. 9 | Comparison of the evolution of the pixel activity level among non-initiating and initiating sites. Simplified pixel activity-level distribution plot for (**a**) a non-initiating S-phase and (**b**–**d**) streak-initiating S-phases from the Fig. 1 sample, and for (**e**) a non-initiating S-phase, and (**f**, **g**) streaking initiating S-phases from Fig. 6 sample. The dashed black lines indicate onset of activity on the IMP surface. The dashed magenta lines indicate streaking corrosion (outside IMP) onsets highlighted in Figs. 4 and 6. The insets show the activity maps of the IMPs that correspond to the plots presented.
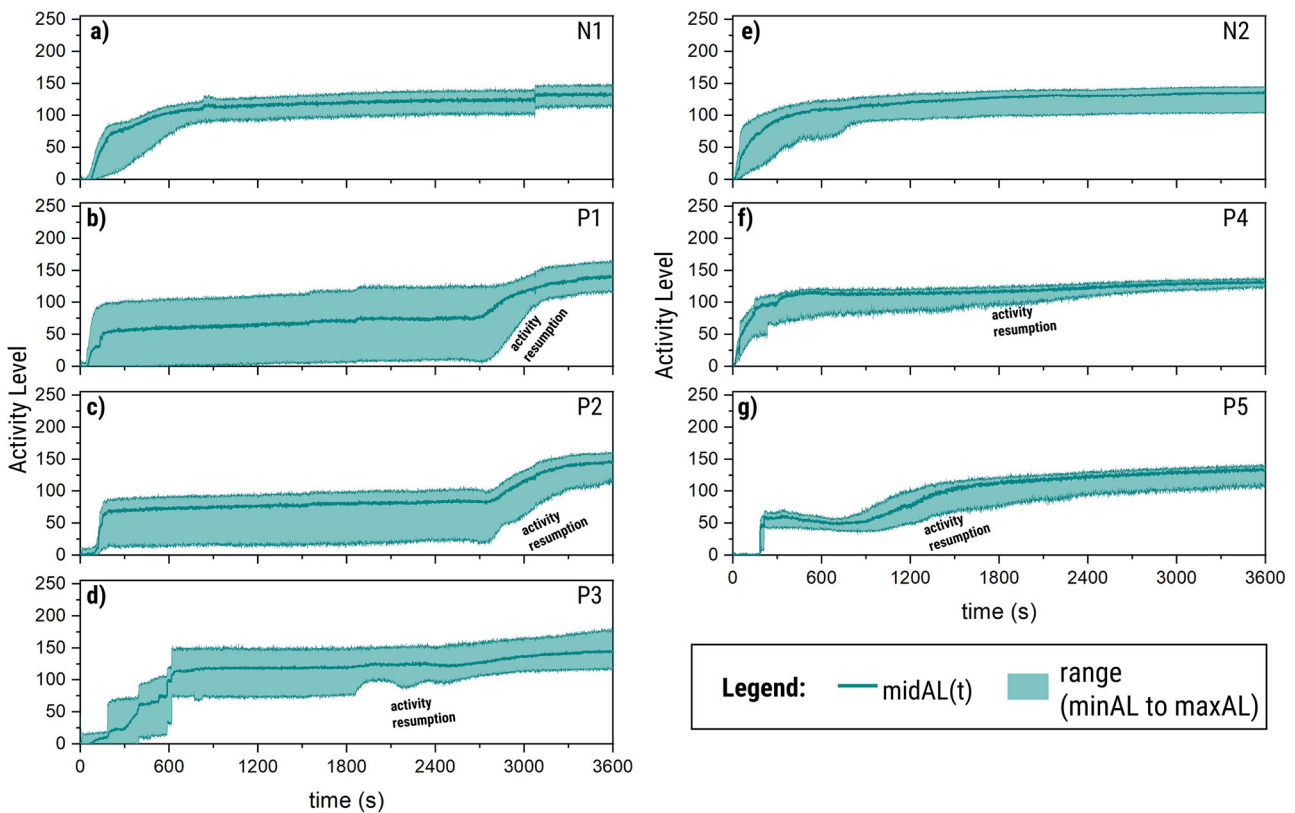
Fig. 10 | Extended simplified pixel activity-level distribution of the particles presented in Fig. 9. The extended simplified pixel activity-level distribution plots show that typical S-phases (**a**, **e**) exhibit quasi-steady behaviour during the first 20 minutes of immersion while streak-initiating IMPs (**b**–**d**, **f**, **g**) show activity increase resumption at a later time.

showed resumed activity increase after overall streaking ended. The termination was observed at around 626 s (Supplementary Fig. S10) and the extended sPADs of the streak-initiating (Fig. 10f, g) and streak-linked IMPs (Fig. 11) show activity increase resumption after this time.

Correlation between open circuit potential transients and streaking corrosion

Figure 12a shows the open circuit potential of the smoothly-polished sample during the first 10 minutes of immersion. OCP measurements for the other
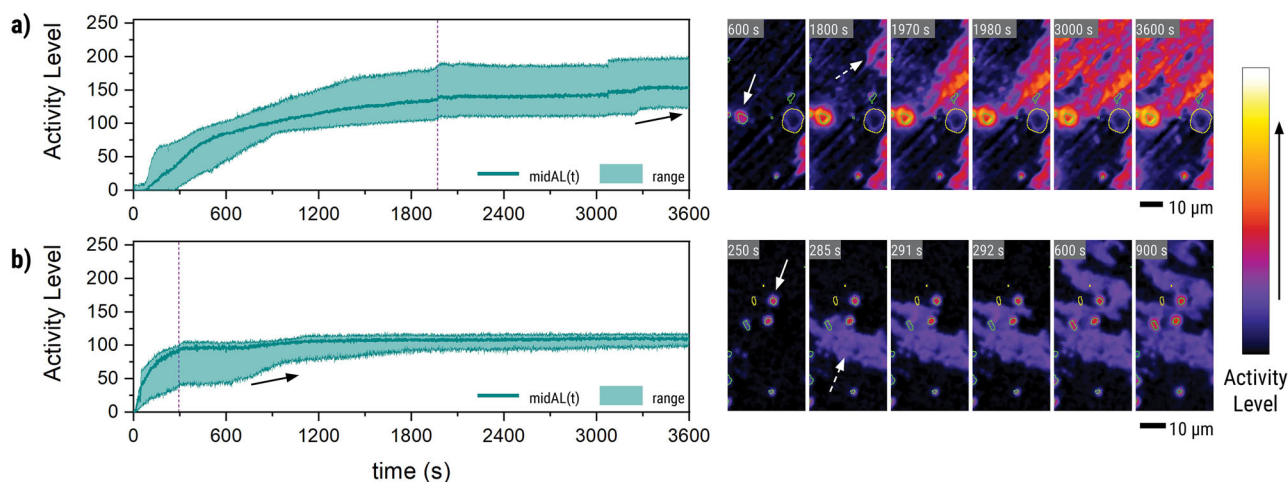
Fig. 11 | Extended simplified pixel activity-level distribution (sPAD) of streak-linked particles. a sPAD of a steak-linked particle from the sample in Fig. 1, and **b** sPAD of a streak-linked particle from the sample in Fig. 6 both show arrest of activity increase and resumption at a later time when they linked to a propagating streak. The dashed magenta line in the simplified pixel activity distribution plots indicates when the propagating streak connected to the IMPs and also mark the beginning of the near-horizontal behaviours.
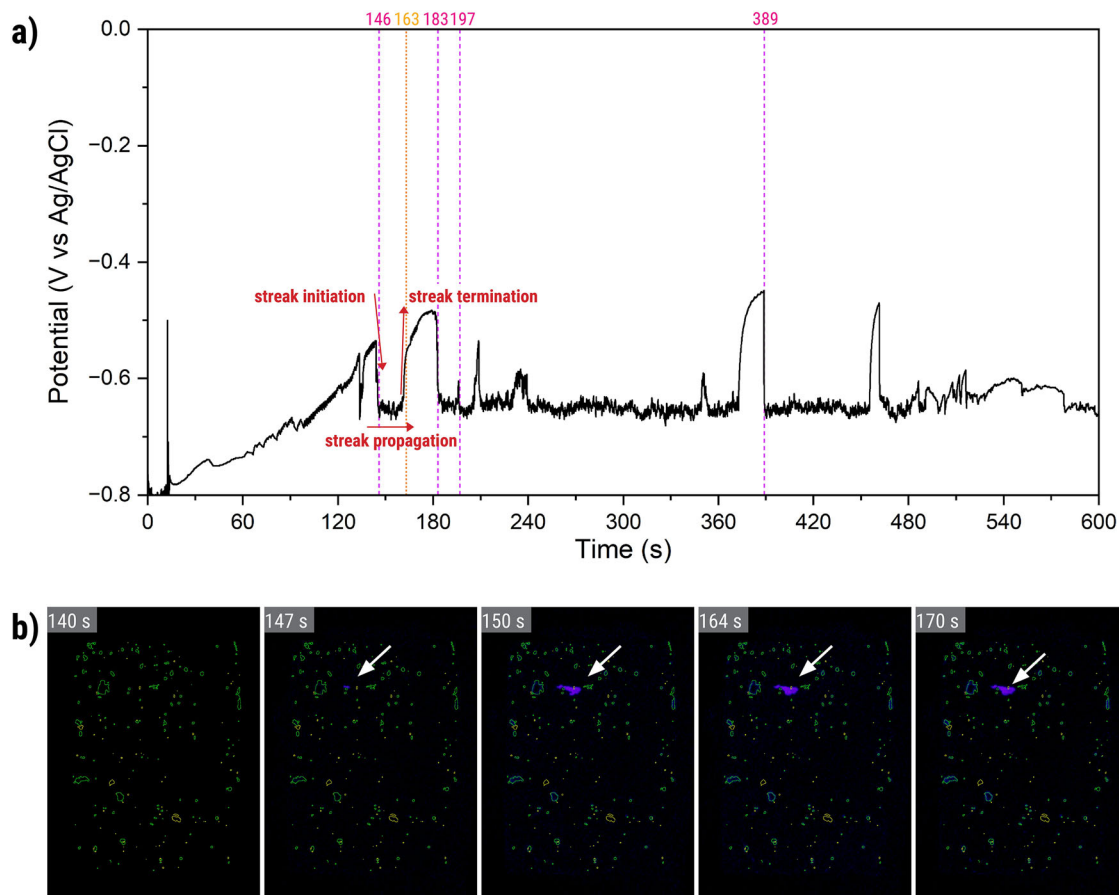

Fig. 12 | Correlation of OCP transients and surface streaking. a Corresponding open circuit potential for the smoothly-polished sample and **b** global activity maps corresponding to the streaking corrosion that initiated at 146 s. The reflected light microscopy image at $t = 140$ s is used as reference to generate these global activity maps so as to isolate the surface processes that gave the electrochemical potential transients at the same period. The duration of the other streaking events on the surface are as follows: 183–197 s (Fig. 6c), 197–208 s (Fig. 6d), 211–374 s (continuation of Fig. 6c, d streaking), 389–457 s (Fig. 6e), 463–627 s (continuation of Fig. 6d, e streaking).

samples are provided in Supplementary Figs. S11–S16 and in Figs. S24 and S25. Increasing OCP values associated with IMP dealloying were observed during the first two minutes of immersion[23,26]. Dashed magenta lines indicate the onset times of streaking events presented in Fig. 6. A sudden OCP

drop is observed around these onset times (i.e., when streak initiated). The drop is then followed by high frequency fluctuations around an OCP value. Once the fluctuations end, a rapid OCP increase is observed coinciding with the end of the streak propagation.
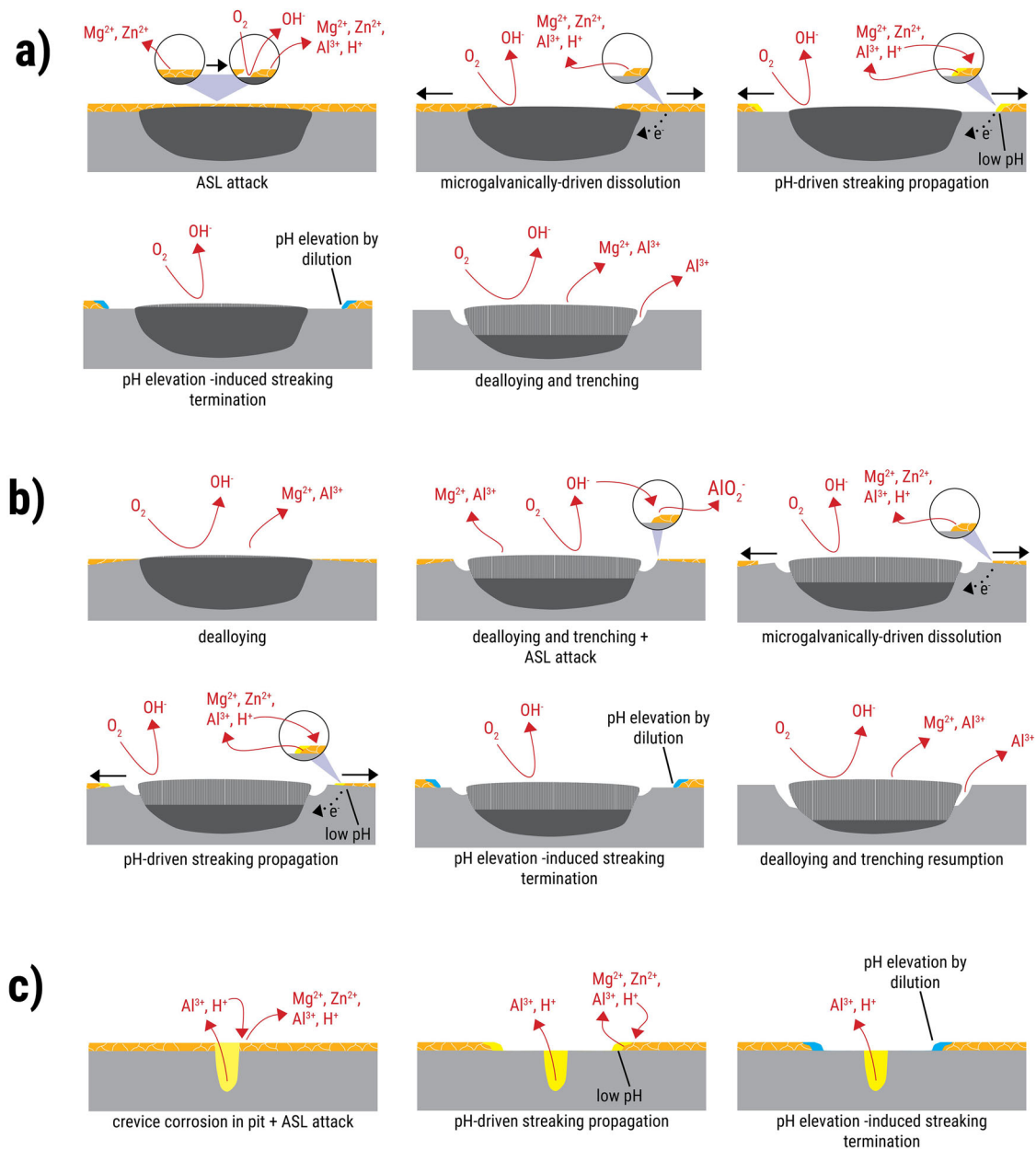
Fig. 13 | Proposed initiation mechanisms for streaking corrosion. a Initiation from an IMP with streaking over the IMP surface, **b** initiation from the trench of an IMP undergoing typical dealloying and trenching, and **c** initiation from pre-existing pits.

Figure 12b shows global activity maps corresponding to the streaking event initiating at 146 seconds. These activity maps use the reflected light microscopy image at 140 seconds as reference for image subtraction. As such, they only highlight surface changes that happened after that point in time. The maps show that the reported streaking event that initiated at P4 (Fig. 6b) was the only major surface event happening from 140 to 170 seconds. The maps also show that the streak propagation from 147 seconds (indicated by white arrows in Fig. 12b) matches the high frequency period observed in the OCP measurements. Absence of changes on the size of the streak between 163 and 170 seconds indicates that streaking terminated at around 163 seconds. At this time, the OCP already increased to pre-drop levels. This suggests that the rapid OCP increase corresponds with the streak approaching termination.

The streaking events at 183, 197, and 389 seconds terminated at 197, 208, and 457 seconds, respectively. As with the streaking at 146 seconds, they also exhibited the sequence of OCP drop, high frequency OCP

fluctuations, and OCP increase. This suggests that this particular OCP transient pattern is characteristic of streaking corrosion. The longest interval during which the pattern was observed is from around 211 to 374 seconds. This corresponds to continuation of the streaking that initiated from area 6 and accounts for forming a major part of the streak in the top section of the sample (Fig. 6a). The streaking corrosion that initiated from area 7 also continued from 463 until 627 s. The same transient pattern is seen during streaking events in the other samples (Supplementary Figs. S11–S13, S24, and S25).

It should be noted that other features are also present in the OCP transients that go beyond the usual sequence of OCP drop, high frequency transients, and OCP increase associated with streaking corrosion. For instance, at around 250 s (Fig. 12a), the high frequency transients exhibited a substantial peaking of the baseline. Another superposition of high frequency transients and baseline drift is also apparent at around 480 s. OCP transients for the other samples also exhibited the characteristic streaking corrosion

transients. However, simultaneous occurrence with other surface events lead to variations in the observed signal. Detailed analysis of these other forms of OCP transients will be covered in another work.

Discussion

Figures 1 and 6 show that localized occurrence of streaking corrosion in OCP conditions is due to preferential initiation on intermetallic particles or pre-existing pits. It is evident though that even among IMPs and pits, streaking initiation happens only with a select few. The few IMPs that served as streaking corrosion triggers can be further grouped based on their *optically-observed behaviour*: (case 1) those where the rapid, streaking-type activity occurred directly over the IMP surface, and (case 2) those where such activity emerged only from the developing trench of an IMP undergoing typical dealloying and trenching. A third case (case 3) includes instances where streaking started from pre-existing pits.

Case 1 (i.e., streaking over IMP surface) includes IMPs that exhibited streaking corrosion behaviour over the IMP surface during the course of its activation that eventually led to streaking corrosion. The streaking over the IMP surface was observed before or around the same time as when streaking propagated beyond the IMP boundary (i.e., streak initiated at IMP). Figure 13a provides the schematic for the proposed mechanism for this case. The streaking over the IMP surface is observed in the activity maps as rapid spread of activity or in the sPADs as a step increase in the activity level. Figure 9 sPADs as well as activity maps from replicate tests (Supplementary Discussion) show that most streak-initiating IMPs belong to this case. P5 showed streaking over the entire IMP surface. Meanwhile, P1, P2, and P3 exhibited partial streaking. Since streaking corrosion is attributed to ASL dissolution[20], streaking over an IMP surface suggests the particle is covered by the ASL (partially or fully). In the absence of the surface layer, the IMPs would have exhibited similar dealloying behaviour as the non-initiating particles (Fig. 9-N1,N2). Non-destructive pre-immersion analysis of the ASL around IMPs and defects is recommended to validate this. Zhao et al.[20] proposed that the dissolution of the surface layer begins with passive layer breakdown, leading to the dissolution of nanograin boundaries. These nanograin boundaries have been previously observed as ~10 nm bands rich in Zn and Mg[11,13,20,25]. Their dissolution then continues through the ASL until the underlying substrate is exposed. This mechanism of ASL dissolution can hypothetically occur on any other section of the sample surface covered by the ASL. This could then trigger streaking corrosion initiation over any part of the AA7075 matrix. Experimentally observed preferential initiation on IMP surfaces here revealed suggest that the underlying particle acts as a trigger for sustained surface layer dissolution. Two possibilities can be considered – the particle caused local variations in the local ASL composition that made it more dissolution-susceptible, or the microgalvanic couple formed between the dissolving Zn- and Mg- rich nanograin boundaries and the underlying IMP promoted sustained dissolution. The second explanation is more likely, given the apparent microgalvanic coupling when IMP activity is temporary inhibited during streaking propagation (Fig. 10) as this indicates that ASL dissolution can interact with the IMPs. Thus, the microgalvanic coupling between the IMP and ASL potentially kickstarts ASL dissolution. Once sufficiently low pH due to hydrolysis of dissolved ions is achieved, the ASL dissolution becomes autocatalytic (i.e., low pH drives dissolution and dissolution sustains low pH) and drives further propagation[12,27].

Case 2 (i.e., streaking from trench around IMP) is characterized by no detectable streaking over the IMP surface prior to streaking corrosion over the matrix (i.e., streaking initiates close to the boundary of the IMP). Instead, the streak-initiating IMP first exhibited dealloying and trenching, similar to the non-initiating IMPs. Figure 13b provides the schematic for the proposed mechanism for this case. This behaviour is only observed with P4 (Fig. 9-P4) and another particle in the replicate tests (Supplementary Discussion). The absence of streaking over the particle suggests that the particle has no ASL cover. Instead, the ASL is situated close to the particle boundary. The IMP dealloying and subsequent trenching potentially generates local chemistry (i.e., high pH) that triggered initial passive layer breakdown of the adjacent ASL. Microgalvanic coupling between the IMP and the ASL then drives propagation of the ASL to areas beyond the high pH vicinity of the IMP. As with case 1, once sufficiently low pH is achieved on the propagation front, the ASL dissolution becomes autocatalytic and drives further streaking corrosion propagation. Notably, the high pH zone close to the dealloying IMP surface potentially explains limited observation of this particular case among the streak-initiating IMPs since the high pH can potentially passivate ASL dissolution. This suggests that for case 2 to proceed, the high pH zone around the IMP should be relatively small, allowing the initial ASL dissolution to produce the acidic environment that will enable the ASL dissolution front to spread out to the matrix. If these conditions are not met, the IMP is more likely to follow typical pathway of localized dealloying and trenching, without initiating streaking.

Case 3 (i.e., streaking from pits) covers streaking corrosion that initiated from a pre-existing pit (Fig. 6d). The initiation is attributed to the aggressive local chemistry, like low pH[28], which develops within the pit likely due to processes such as crevice corrosion[29]. If the pit is in close proximity to an ASL, the low pH can trigger sustained ASL dissolution (i.e., autocatalytic ASL dissolution) and lead to streaking corrosion propagation (Fig. 13b)[12,27].

The development of sustained ASL dissolution in all of the cases potentially accounts for the observed OCP drop when streaking corrosion is initiating (Fig. 12a). This is consistent with previous reports of streaking corrosion being a dissolution process[11,12]. Huang et al. proposed that the ASL dissolution will continue propagating as long as the pH is low enough to drive breakdown ahead of the streak[12,21]. The depth of attack stemming from streaking corrosion over the matrix appears to be limited though which is why the activity levels associated with propagating streaks remain low (i.e., purple colour in the activity maps). The low activity level of the streaked areas also show minimal surface damage – shallower than trenching around most IMPs (Figs. 5, 8). Even though the corrosion attack is shallow, its propagation can undermine adhesion between protective coatings and the AA7075 substrate. This can then lead to issues such as filiform corrosion[15,30]. The streaking propagation also results to the high-frequency fluctuations around an OCP baseline (Fig. 12a). It should be noted that the high-frequency fluctuations happened after an OCP drop during streaking initiation.

The propagating ASL dissolution can couple with the IMP surface, leading to slower dealloying rates. This is seen as near-horizontal profiles in the sPADs (Figs. 9, 10) following streaking initiation. The near-horizontal profiles confirm that the degree of change on the IMP surface is not increasing which suggests that the dealloying of the particle is not progressing. This apparent inhibition is attributed to the Zn and Mg in the ASL[11,13,20,25] acting as sacrificial anodes[31,32] which temporarily limit dissolution of less noble components of the IMPs (e.g., Al). Once the streaking stops, the sacrificial anode effect ends, and IMP dealloying resumes (Figs. 10, 11). The streaking corrosion termination has previously been attributed to the pH at the front not being low enough due to dilution with the bulk electrolyte[12,21]. However, there is also the possibility that streaking ceases because the compositional differences driving the phenomenon are no longer present — specifically, that the ASL has fully dissolved. As such, further experimentation is recommended to determine the mechanism behind the termination of streaking corrosion. Nonetheless, the termination of the rapid anodic dissolution of the surface layer also leads to a return of the potential to the pre-streaking state (i.e., OCP increase) wherein cathodic reactions (e.g., oxygen reduction reaction) on the IMP surfaces are balanced by dissolution of less noble components on the intermetallic particle and on the trenches (Fig. 12a). The observed OCP increase after streaking termination can thus be interpreted as the system's relaxation after being perturbed by the streaking corrosion.

Methods

Commercial grade bare AA7075-T6 (Kaiser Aluminium, rolled thickness = 3 mm) was used for the corrosion tests. Micropillars were produced from the metal sheets and embedded in cold-curing epoxy as

reported elsewhere[23,24,26]. The resulting embedded sample had an exposed metal surface area of approximately $260 \times 170~\mu m^2$. The exposed area is along the rolling plane of the alloy. The sample was repolished for each new corrosion test. The solution used for the corrosion tests was a 0.05 M NaCl aqueous solution (> 98% purity NaCl in "Millipore Elix 3 UV" treated water).

Prior to immersion in the corrosive solution, the sample surface was ground with SiC sandpaper from 320 to 4000 grit and then polished to 0.25 μm with diamond paste. For samples subjected to pre-exposure microstructure analysis, location and spot composition of IMPs and defects (e.g., pre-existing pits) were determined using SEM-EDX (JEOL JSM-7500F field emission scanning electron microscope coupled with energy dispersive X-ray spectroscopy) operated in back-scattered electron mode. The SEM images were used to generate the microstructure map of the sample surface. Right after SEM-EDX analysis, the sample was quickly repolished with 0.25 μm diamond paste and washed with ethanol before the immersion tests. The sample was then placed in the in situ optical-electrochemical setup composed of an electrochemical cell (redox.me Raman electrochemical flow cell) and a reflected microscope (Dinolite AM7515MT4A, ~10 pixel μm^{-2}) operating in brightfield mode for in-situ acquisition of images of the surface during immersion[23,24]. The sample served as the working electrode and a Ag/AgCl(3 M KCl) reference electrode integrated into the electrochemical cell was used as the reference electrode. The OCP measurements were acquired using an Ivium CompactStat.h potentiostat. The immersion tests were conducted inside a Faraday cage to prevent interference from external resources. The cage is also equipped with blinds to remove the effect of ambient light changes on in situ imaging. Image capture and potential measurements were initiated prior to the injection of the electrolyte into the cell to enable collection of data from the very start of exposure. The sample was immersed in 4.5 mL of the electrolyte for 2 hours. Post-immersion analysis of the sample was performed with SEM-EDX. It is noted that in some cases, the post-immersion SEM images can also be used to generate the microstructure map of the sample surface.

Detailed discussion of our image analysis protocol for studying local changes in the sample surface is presented in our previous work[24]. Our analysis focuses on detecting and quantifying the changes which happened during immersion by implementing image subtraction on our pre-processed (i.e., conversion to grayscale, recursive realignment) optical images. It is noted that the images have been converted to grayscale, as such each pixel has an associated gray-level. With the imaging mode used (i.e., brightfield imaging), local corrosion is generally observed as pixel darkening. This happens because local corrosion changes the surface by either wearing some parts away or adding corrosion products, both of which makes the surface rougher. A rougher surface scatters more light away, causing the pixels to look darker in the image. The subtraction was generally performed with respect to the first image acquired during immersion (i.e., image @ 0 s of immersion – image @ x s of immersion) unless otherwise stated. This subtraction process generated the global activity map (GAM) for the sample at time x. The GAM shows change in gray-level of individual pixels (i.e., pixel activity). A built-in ImageJ look-up table (i.e., Fire) was used to recolour the GAMs to enable easier visualisation of the magnitude of the changes. The activity levels depicted in the GAMs range from 0 to 255, with 0 indicating no change with respect to the initial condition. A threshold can be applied to the GAM to balance signal to noise ratio and quantify the affected area percentage (Eq. 1). Cross-referencing of the evolution of surface activity with the microstructure was achieved by overlaying the microstructure map obtained through SEM on to the GAMs. The map can then be used to isolate specific areas of the GAM for analysing local surface changes (i.e., IMP level). The changes were visualized through simplified pixel activity level distribution (sPAD) plots[24]. These plots present the maximum (maxAL), median (midAL), and minimum (minAL) activity levels as a function of time for the set of pixels on the IMP surface. The midAL is

useful for looking at the overall behaviour of the surface. Meanwhile, the maxAL and the midAL provide additional sensitivity to changes during early- and late-stage corrosion, respectively.

$$\text{Affected area}\% = \frac{\text{No.of pixels with activity level} \geq \text{threshold}}{\text{Total number of pixels in sample surface}} \times 100\%$$

(1)

Data availability

Code availability

References

1. Kosari, A. et al. Dealloying-driven local corrosion by intermetallic constituent particles and dispersoids in aerospace aluminium alloys. *Corros. Sci.* **177**, 108947 (2020).
2. Kumar, A., Chaudhari, G. P. & Nath, S. K. Correlation of microstructure with corrosion performance in high zinc 7068 aluminum alloy aged using different T6 conditions. *Mater. Charact.* **191**, 112133 (2022).
3. Ayer, R., Koo, J. Y., Steeds, J. W. & Park, B. K. Microanalytical study of the heterogeneous phases in commercial Al-Zn-Mg-Cu alloys. *Metall. Trans. A* **16**, 1925–1936 (1985).
4. Zhu, Y., Sun, K. & Frankel, G. S. Intermetallic phases in aluminum alloys and their roles in localized corrosion. *J. Electrochem Soc.* **165**, C807–C820 (2018).
5. Kosari, A. et al. In-situ nanoscopic observations of dealloying-driven local corrosion from surface initiation to in-depth propagation. *Corros. Sci.* **177**, 108912 (2020).
6. Hashimoto, T. et al. Investigation of dealloying of S phase (Al2CuMg) in AA 2024-T3 aluminium alloy using high resolution 2D and 3D electron imaging. *Corros. Sci.* **103**, 157–164 (2016).
7. Mallinson, C. F. et al. The localised corrosion associated with individual second phase particles in AA7075-T6: A study by SEM, EDX, AES, SKPFM and FIB-SEM. *Mater. Corros.* **68**, 748–763 (2017).
8. Andreatta, F., Terryn, H. & de Wit, J. H. W. Effect of solution heat treatment on galvanic coupling between intermetallics and matrix in AA7075-T6. *Corros. Sci.* **45**, 1733–1746 (2003).
9. Liu, L. L., Pan, Q. L., Wang, X. D. & Xiong, S. W. The effects of aging treatments on mechanical property and corrosion behavior of spray formed 7055 aluminium alloy. *J. Alloy. Compd.* **735**, 261–276 (2018).
10. Huo, W. et al. Simultaneously enhanced mechanical strength and inter-granular corrosion resistance in high strength 7075 Al alloy. *J. Alloy. Compd.* **781**, 680–688 (2019).
11. Wang, S. S., Jiang, J. T., Fan, G. H., Frankel, G. S. & Zhen, L. Effects of long-term natural aging on the altered surface layer on an Al-Zn-Mg-Cu alloy and on corrosion properties. *Electrochim. Acta* **266**, 34–42 (2018).
12. Huang, R. S., Lin, C. J. & Isaacs, H. S. A difference-imaging technique used to study streaking corrosion of aluminum alloys AA7075 and AA8006 in chloride solution. *Electrochem. Solid-State Lett.* **9**, B11 (2006).
13. Liu, Y. et al. Corrosion behaviour of mechanically polished AA7075-T6 aluminium alloy. *Surf. Interface Anal.* **42**, 185–188 (2010).

14. Seong, J., Yang, F., Scheltens, F., Frankel, G. S. & Sridhar, N. Influence of the Altered Surface Layer on the Corrosion of AA5083. *J. Electrochem Soc.* **162**, C209–C218 (2015).

15. Liu, Y. et al. Influence of near-surface deformed layers on filiform corrosion of AA3104 aluminium alloy. *Surf. Interface Anal.* **45**, 1553–1557 (2013).

16. Afseth, A., Nordlien, J. H., Scamans, G. M. & Nisancioglu, K. Influence of heat treatment and surface conditioning on filiform corrosion of aluminium alloys AA3005 and AA5754. *Corros. Sci.* **43**, 2359–2377 (2001).

17. Afseth, A., Nordlien, J. H., Scamans, G. M. & Nisancioglu, K. Effect of thermo-mechanical processing on filiform corrosion of aluminium alloy AA3005. *Corros. Sci.* **44**, 2491–2506 (2002).

18. Ambat, R., Davenport, A. J., Afseth, A. & Scamans, G. Electrochemical behavior of the active surface layer on rolled aluminum alloy sheet. *J. Electrochem Soc.* **151**, B53 (2004).

19. Liu, B., Zhang, X., Zhou, X., Hashimoto, T. & Wang, J. The corrosion behaviour of machined AA7150-T651 aluminium alloy. *Corros. Sci.* **126**, 265–271 (2017).

20. Zhao, Z. & Frankel, G. S. On the first breakdown in AA7075-T6. *Corros. Sci.* **49**, 3064–3088 (2007).

21. Huang, R. S., Lin, C. J. & Isaacs, H. S. Measuring streaking rates of an Al–Zn alloy using a difference imaging technique. *Corros. Sci.* **48**, 1867–1873 (2006).

22. Wang, S.-S. et al. Mechanism of Localized Breakdown of 7000 Series Aluminum Alloys. *J. Electrochem Soc.* **160**, C493–C502 (2013).

23. Olgiati, M., Denissen, P. J. & Garcia, S. J. When all intermetallics dealloy in AA2024-T3: quantifying early stage intermetallic corrosion kinetics under immersion. *Corros Sci* https://doi.org/10.1016/j.corsci.2021.109836 (2021).

24. Mopon, M., Mol, A. & Garcia, S. J. Effect of delayed inhibitor supply on AA2024-T3 intermetallic activity: A local in situ analysis with reflected microscopy. *Corros. Sci.* **230**, 111910 (2024).

25. Zhao, Z. & Frankel, G. S. Surface layer dissolution kinetics of aluminum alloy 7075 in various tempers. *Corrosion* **63**, 613–624 (2007).

26. Homborg, A. M., Olgiati, M., Denissen, P. J. & Garcia, S. J. An integral non-intrusive electrochemical and in-situ optical technique for the study of the effectiveness of corrosion inhibition. *Electrochim. Acta* **403**, 139619 (2022).

27. Isaacs, H. S., Scheffey, C. & Huang, R. The location of events producing potential transients during pitting of freely corroding Al and its alloys. *ECS Trans.* **11**, 1–12 (2008).

28. Xiao, J. & Chaudhuri, S. Predictive modeling of localized corrosion: An application to aluminum alloys. *Electrochim. Acta* **56**, 5630–5641 (2011).

29. Li, Y., Tang, Y., Liu, X. & Li, Y. Insight into the crevice corrosion mechanism of AA7075-T651 high-strength aluminum alloys in neutral nitrate solution: The effect of Cl−. *Mater. Corros.* **75**, 1373–1388 (2024).

30. Liu, B., Zhou, X. & Zhang, X. Filiform corrosion behaviour on machined AA7150 aluminium alloy. *Trans. Nonferrous Met. Soc. China* **30**, 2056–2066 (2020).

31. Korjenic, A., Romanovskaia, E. & Scully, J. R. Spatially resolved assessment and analysis of Al-Zn, Mg, and Mg/Al-Zn metal-rich primers applied to AA 7075-T651 in full immersion. *J. Electrochem Soc.* **171**, 091505 (2024).

32. Vu Dinh, T. et al. On the miniaturised sacrificial protection achieved by surface precipitation in aluminium alloys. *Corros. Sci.* **145**, 67–79 (2018).

Acknowledgements

Author contributions
The study was conceived by M.M., A.M. and S.G. M.M. performed sample preparation, experiments, data acquisition, and analysis under the supervision of S.G. and A.M. All authors discussed the data interpretation. M.M. wrote the paper's first draft, revised by all. All authors approved the final version.

Competing interests
The authors declare no competing interests.

Additional information
Supplementary information The online version contains supplementary material available at https://doi.org/10.1038/s41529-025-00631-5.

Correspondence and requests for materials should be addressed to Marlon Mopon Jr. or Santiago J. Garcia.

Reprints and permissions information is available at http://www.nature.com/reprints

Publisher's note Springer Nature remains neutral with regard to jurisdictional claims in published maps and institutional affiliations.